# DOCK8 is expressed in microglia, and it regulates microglial activity during neurodegeneration in murine disease models

**Kazuhiko Namekata[‡], Xiaoli Guo[‡], Atsuko Kimura[‡], Nobutaka Arai[§], Chikako Harada[‡], and ⊙ Takayuki Harada[‡1]**

*From the [‡]Visual Research Project, Tokyo Metropolitan Institute of Medical Science, Tokyo 156-8506, Japan and [§]Brain Pathology Research Center, Tokyo Metropolitan Institute of Medical Science, Tokyo 156-8506, Japan*

Edited by Roger J. Colbran

Dedicator of cytokinesis 8 (DOCK8) is a guanine nucleotide exchange factor whose loss of function results in immunodeficiency, but its role in the central nervous system (CNS) has been unclear. Microglia are the resident immune cells of the CNS and are implicated in the pathogenesis of various neurodegenerative diseases, including multiple sclerosis (MS) and glaucoma, which affects the visual system. However, the exact roles of microglia in these diseases remain unknown. Herein, we report that DOCK8 is expressed in microglia but not in neurons or astrocytes and that its expression is increased during neuroinflammation. To define the role of DOCK8 in microglial activity, we focused on the retina, a tissue devoid of infiltrating T cells. The retina is divided into distinct layers, and in a disease model of MS/optic neuritis, DOCK8-deficient mice exhibited a clear reduction in microglial migration through these layers. Moreover, neuroinflammation severity, indicated by clinical scores, visual function, and retinal ganglion cell (RGC) death, was reduced in the DOCK8-deficient mice. Furthermore, using a glaucoma disease model, we observed impaired microglial phagocytosis of RGCs in DOCK8-deficient mice. Our data demonstrate that DOCK8 is expressed in microglia and regulates microglial activity in disease states. These findings contribute to a better understanding of the molecular pathways involved in microglial activation and implicate a role of DOCK8 in several neurological diseases.

Dedicator of cytokinesis 8 (DOCK8)[2] is a guanine nucleotide exchange factor (GEF) that belongs to the DOCK-C subfamily of the DOCK family (1, 2). DOCK proteins activate Rho GTPases Rac1 and/or Cdc42, and their biological functions include regulation of cell morphology, migration, growth, and adhesion (3–5). Research into DOCK8 was accelerated in 2009 when its loss-of-function mutations in humans were reported to be responsible for a combined immunodeficiency (6–9) in which there is a defect in B-cell and T-cell function. Indeed, DOCK8 is highly expressed in B cells and T cells, and much research was focused on the role of DOCK8 in the immune system. DOCK8 is required for intrinsic function of B cells (10), and its role in the TLR–MyD88 signaling pathway as an adaptor protein suggests that it also acts in a GEF-independent manner (11). It plays a key role in the survival, function, and morphological integrity of CD8^{+} T cells and natural killer T cells (12–14) and regulation of cytokine production by CD4^{+} T cells (15). Moreover, DOCK8 is essential for T-cell receptor–driven actin polymerization (16), and it regulates migration of dendritic cells (17, 18). All of these findings indicate important roles of DOCK8 in the immune system. Conversely, DOCK8 mutations are associated with autism, mental retardation, and neuroblastoma (19–21), indicating that DOCK8 may also be involved in neurological disorders. However, the role of DOCK8 in the central nervous system (CNS) is unknown. In fact, there have not been any reports demonstrating that DOCK8 is expressed in cells in the CNS, including microglia. Microglia are the resident immune cells of the CNS. Resting microglia show ramified morphology, and these microglia survey the local environment constantly for any injuries. In response to CNS insults, resting microglia retract their processes and adopt reactive or ameboid forms. These reactive microglia are implicated in various brain diseases, and so they are a potential therapeutic target (22–25).

One example of a disease in which microglia are implicated is multiple sclerosis (MS), a chronic autoimmune disease of the CNS characterized by demyelination and degeneration of axons, resulting in a variety of symptoms, including tingling, numbness, fatigue, and cognitive and visual impairment. Experimental autoimmune encephalomyelitis (EAE) is the most commonly used animal model of MS, and it has provided useful information on understanding this complex disease (26, 27). Although the main pathogenic players in MS are proinflammatory lymphocytes (28–32), we have previously reported a role of glial cells in EAE (33, 34), and activated microglia are

**SASBMB**

*J. Biol. Chem.* (2019) 294(36) 13421–13433  **13421**
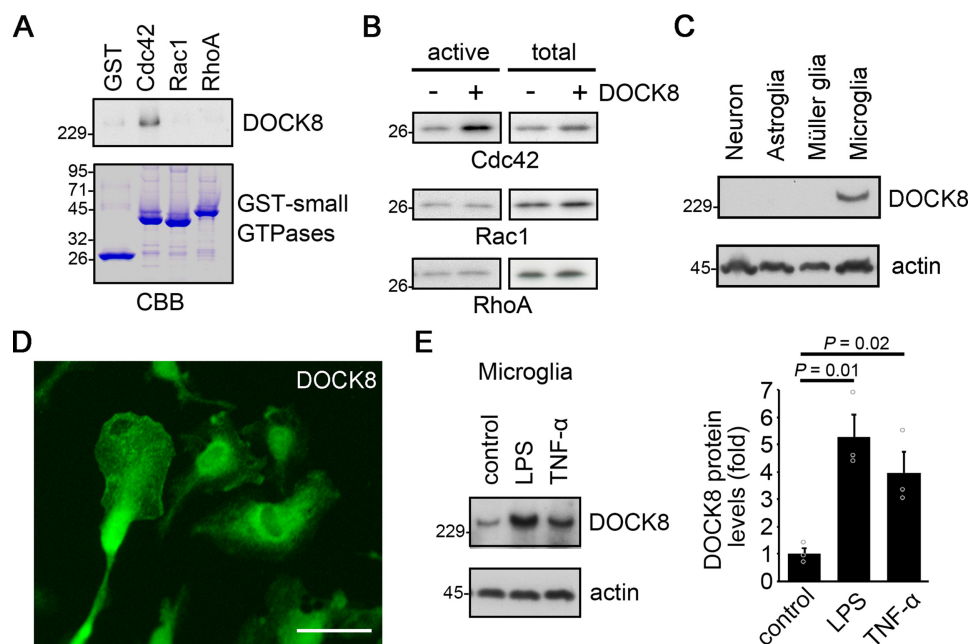
**Figure 1. DOCK8 is expressed in microglia and is up-regulated by proinflammatory cytokines.** *A*, DOCK8 binds specifically to Cdc42. GST-Cdc42, GST-Rac1, GST-RhoA, and GST alone were mixed and incubated with lysates of COS-7 cells overexpressing DOCK8. GST-small GTPases were isolated by a pulldown assay, and bound DOCK8 was detected by immunoblot analysis. *B*, DOCK8 promotes GTP loading of Cdc42. Myc-tagged Cdc42, Rac1, and RhoA were transfected into COS-7 cells with DOCK8. After 24 h of transfection, GTP-Cdc42 was pulled down from lysates with GST-CRIB, GTP-Rac1 was pulled down with GST-CRIB, and GTP-RhoA was pulled down with GST-Rhotekin. Each small G protein was detected by immunoblot analysis. *C*, immunoblot analysis of DOCK8 in primary cultured neurons, astroglia, Müller glia, and microglia. DOCK8 is only expressed in microglia. *D*, immunostaining of DOCK8 in primary cultured microglia. DOCK8 was diffusely expressed in the cytoplasm of microglia. *E*, immunoblot analysis of DOCK8 in primary cultured microglia stimulated with LPS (10 ng/ml) or TNFα (50 ng/ml) for 24 h. Both LPS and TNFα up-regulated DOCK8 expression levels. *Error bars* represent S.E. (*n* = 3) and data were analyzed by a Student's *t* test. *Scale bar*, 20 μm. *CBB*, Coomassie Brilliant Blue.

found in the brain of MS patients (35–37). Interestingly, minocycline, a tetracycline antibiotic that prevents microglial activation, is in clinical trials for treatment of MS and producing promising results (38), further supporting the role of microglia in MS. As mentioned above, a role of DOCK8 in myeloid and lymphoid cells has been reported; however, a role of microglial DOCK8 in neuroinflammation is unknown.

Microglial activation is observed in various retinal degenerative diseases, including glaucoma (39). Glaucoma is a neurodegenerative disease of the eye, and it is one of the major causes of blindness worldwide. The pathology of glaucoma is characterized by progressive degeneration of the optic nerve and retinal ganglion cells (RGCs), which are found in the retina. The optic nerve injury (ONI) model is an experimentally induced model of glaucoma and is a good model for investigating microglial responses as their activation is clearly demonstrated (40–43). Also, this model is particularly useful for studying a role of microglial DOCK8 in disease as T cells do not infiltrate into the retina, allowing the examination of the role of DOCK8 in microglia independently of DOCK8 in T cells, unlike in the EAE model. Currently, information on microglial dynamics in the retina is limited due to a lack of tools for visualizing and capturing morphological and functional changes of these cells in diseased states. Therefore, a new method to visualize changes in microglial morphology would be desired to further understand the role of microglia in disease states.

In this study, we examined whether DOCK8 is expressed in neural cells and determined whether microglial DOCK8 plays a role in neurodegenerative diseases using mouse MS and glaucoma models. We focused on the retina, a tissue that is structured in distinct layers, allowing monitoring of migration of microglia easily and where the pathology is not associated with infiltrating T cells. We visualized morphology of microglia in reconstructed 3D images to demonstrate microglial activation during healthy and disease states.

## Results

### DOCK8 expression is increased in microglia during neuroinflammation

First, we examined the interaction of DOCK8 with Cdc42, Rac1, and RhoA. Immunoblot analysis revealed that DOCK8 binds to Cdc42 but not to Rac1 or RhoA (Fig. 1*A*). Consistently, DOCK8 possessed GEF activity for Cdc42 but not for Rac1 or RhoA (Fig. 1*B*). These data suggest that DOCK8 selectively activates Cdc42.

Cdc42 plays a role in the migration of inflammatory cells (44), and therefore, we investigated whether DOCK8 is involved in neuroinflammation. For this, we first assessed DOCK8 expression in various cell types in the CNS, including neurons, astroglia, retinal Müller glia, and microglia. Immunoblotting analyses revealed that DOCK8 expression was found in microglia but not in any other cell types we tested (Fig. 1*C*). Furthermore, immunocytochemical analysis revealed that DOCK8 was expressed diffusely in the cytoplasm of microglia (Fig. 1*D*). Because DOCK8 plays important roles in immune responses (10–12, 17), we investigated whether inflammatory mediators affect DOCK8 expression levels in microglia. We
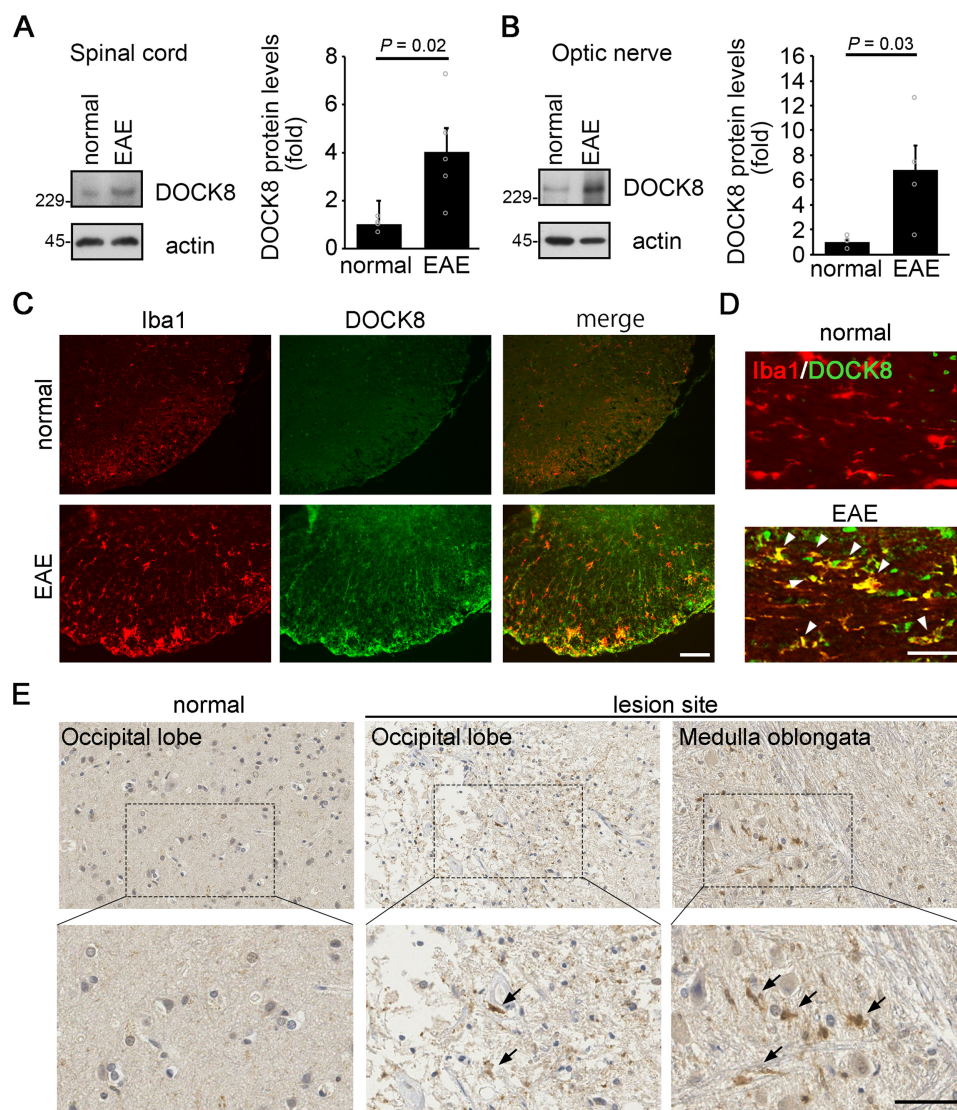
**Figure 2. DOCK8 expression is up-regulated in mouse and human neuroinflammation.** *A* and *B*, immunoblot analysis of DOCK8 in the spinal cord (*A*) and optic nerve (*B*) of WT EAE mice. The DOCK8 expression is increased in the EAE spinal cord and optic nerve. *Error bars* represent S.E. (*n* = 4 mice for normal and *n* = 5 mice for EAE in *A*; *n* = 4 mice for normal and EAE in *B*) and data were analyzed by a Mann–Whitney *U* test. *C* and *D*, double immunostaining of the white matter of the spinal cord (L1–L3) (*C*) and optic nerve (*D*) of WT EAE mice using anti-Iba1 (*red*) and anti-DOCK8 (*green*) antibodies. *Arrowheads* indicate increased expression of DOCK8 in microglia in the optic nerve of WT EAE mice. *E*, immunostaining of the paraffin sections of the occipital lobe and medulla oblongata from a patient with MS using an anti-DOCK8 antibody; "normal" indicates an area from the MS patient without a lesion. In the lesion site, DOCK8-positive cells were detected, and some of them seemed to show microglia-like morphology (*arrows*). *Scale bars*, 100 μm (*C*), and 50 μm (*D* and *E*).

found that DOCK8 expression levels in primary cultured microglia were drastically up-regulated by stimulation with lipopolysaccharide (LPS) and tumor necrosis factor-α (TNFα) (Fig. 1*E*). To confirm whether this is also true *in vivo*, we investigated DOCK8 expression levels in the spinal cord and optic nerve in EAE mice. Western blotting analyses demonstrated that DOCK8 expression levels were significantly increased in both the spinal cord and optic nerve of EAE mice compared with those of normal mice (Fig. 2, *A* and *B*). Double-immuno-histochemical staining revealed that DOCK8 expression was strongly increased in the EAE spinal cord and colocalized with Iba1 (Fig. 2, *C* and *D*) and TREM2 (Fig. S1), a transmembrane glycoprotein that has been shown to be linked to DOCK8 by gene network analysis in Alzheimer's disease brain (45). Together, these results suggest that DOCK8 expression in microglia is increased during neuroinflammation.

We also examined whether DOCK8 expression is increased in human MS. Immunohistochemical analysis of the occipital lobe and medulla oblongata revealed that DOCK8-immunopo-sitive cells were drastically increased in the lesion site compared with the nonlesion site of human MS tissues (Figs. 2*E* and S2). Moreover, some DOCK8-positive cells in the lesion site appeared with microglia-like morphology (Fig. 2*E*, *arrows*). These results demonstrated that DOCK8 expression is increased during neuroinflammation in both mice and humans.

### DOCK8 is critical for activation of microglia in EAE

To investigate a role of microglial DOCK8 during neuroinflammation, we generated DOCK8-deficient (*DOCK8⁻/⁻*) mice. Primary cultured microglia from *DOCK8⁻/⁻* mice showed cell morphology similar to that from WT mice (Fig. 3*A*), and expression levels of actin-regulating proteins were not
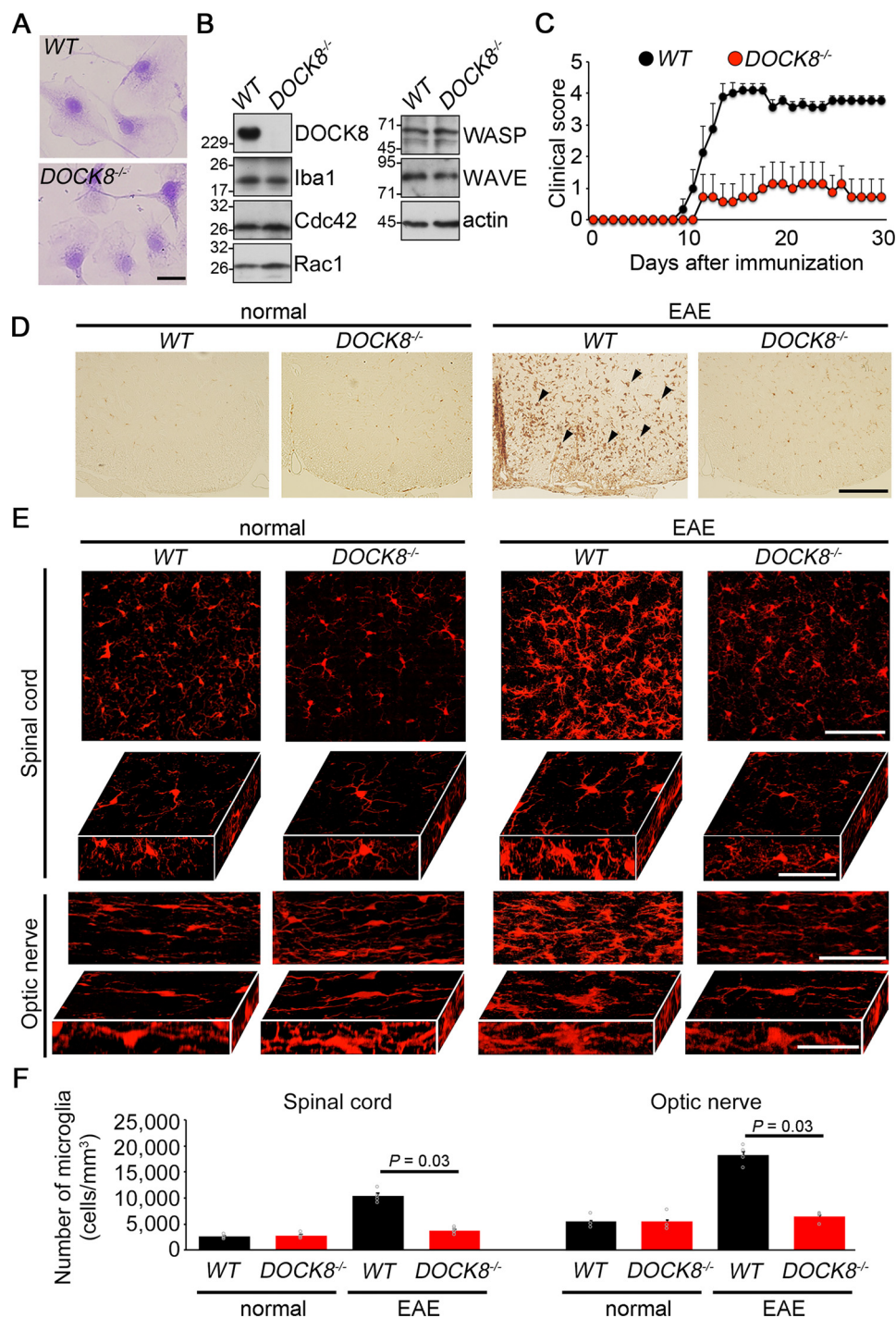
**Figure 3. DOCK8 deficiency reduces proliferation of microglia in EAE mice.** *A*, cultured microglia from WT and *DOCK8$^{-/-}$* mice were visualized by crystal violet staining. No abnormal morphology is detected in *DOCK8$^{-/-}$* microglia. *B*, immunoblot analysis of actin-regulating proteins in primary cultured microglia from WT and *DOCK8$^{-/-}$* mice. DOCK8 deficiency does not affect the level of total protein expression of actin-regulating proteins. *C*, clinical scores of WT and *DOCK8$^{-/-}$* EAE mice ($n = 9$ for WT; $n = 7$ for *DOCK8$^{-/-}$*). The severity of EAE symptoms is reduced in *DOCK8$^{-/-}$* EAE mice. *D*, immunohistochemistry of paraffin sections using an anti-Iba1 antibody in the white matter of spinal cord (L1–L3) of WT and *DOCK8$^{-/-}$* EAE mice. EAE up-regulates Iba1-positive cells in WT mice but not in *DOCK8$^{-/-}$* mice. *E*, 2D and 3D images of microglia immunostained with an anti-Iba1 antibody in the white matter of the spinal cord (L1–L3) and optic nerve of WT and *DOCK8$^{-/-}$* EAE mice. Morphological changes in microglia representing the activation state are detected in WT EAE mice but not in *DOCK8$^{-/-}$* EAE mice. *F*, number of microglia in the spinal cord and optic nerve. The number of microglia in *DOCK8$^{-/-}$* EAE mice is much lower than that in WT EAE mice. *Error bars* represent S.E. (spinal cord, $n = 4$ mice for WT and *DOCK8$^{-/-}$* normal and WT EAE and $n = 5$ mice for *DOCK8$^{-/-}$* EAE; optic nerve, $n = 3$ mice for WT and *DOCK8$^{-/-}$* normal and $n = 4$ mice for WT and *DOCK8$^{-/-}$* EAE) and data were analyzed by a Mann–Whitney *U* test. *Scale bars*, 10 $\mu$m (*A*); 100 $\mu$m (*D*), 100 $\mu$m for the spinal cord and 50 $\mu$m for the optic nerve (2D image) and 50 $\mu$m for the spinal cord and 25 $\mu$m for the optic nerve (*box* image) (*E*).

altered by a DOCK8 deficiency (Fig. 3*B*). We induced EAE in WT and *DOCK8$^{-/-}$* mice and found that DOCK8 deficiency ameliorated EAE symptoms (Fig. 3*C*). Histopathological analysis with luxol fast blue and hematoxylin and eosin staining demonstrated that demyelination and activation of astrocytes were reduced in the spinal cord of *DOCK8$^{-/-}$* EAE mice (Fig. S3).

Moreover, an increased number of microglial cells are detected in WT EAE mice but not in $DOCK8^{-/-}$ EAE mice (Fig. 3D). To assess changes in microglial morphology *in vivo* in detail, we developed a simple method to create a 3D image reconstruction of tissues to allow visualization of a 3D image of microglia using simultaneous application of the tissue clearing technique and immunostaining. This method captured the differences in microglial morphology among various tissues (retina, optic nerve, and spinal cord) and among different layers (the inner plexiform layer (IPL) and the outer plexiform layer (OPL)) within the retina (Fig. S4). EAE-induced changes in the microglial number were clearly demonstrated by the 3D image reconstruction of the spinal cord (Fig. 3E). The number of microglia in the spinal cord and optic nerve of WT EAE mice was increased by more than 3–4 times compared with that of normal WT mice, whereas the number of microglia in $DOCK8^{-/-}$ EAE mice was similar to that of normal WT mice (Fig. 3F). Immunostaining with a Ki67 antibody revealed that microglial cell proliferation was increased in the spinal cord of WT EAE mice but not in $DOCK8^{-/-}$ EAE mice (Fig. S5), whereas in the retina microglial cell proliferation was not detectable in WT EAE mice (Fig. S6). In addition, many microglia with de-ramified morphology were found in both the spinal cord and optic nerve from WT EAE mice but not from $DOCK8^{-/-}$ EAE mice (Fig. 3, *E and F*, and Movies S1 and S2). Taken together, these results demonstrate that DOCK8 deficiency suppresses microglial activation and decreases the number of microglia in the spinal cord and optic nerve during EAE.

### Role of microglial DOCK8 in retinal degeneration in EAE

Our observations so far suggest that DOCK8 deficiency reduces microglial activation and ameliorates EAE severity. However, considering that in mice DOCK8 deficiency and DOCK8 mutation with abolished GEF activity for Cdc42 activation reduce T-cell infiltration into the CNS and affect T-cell function (Fig. S7) (46), microglial activity might be suppressed due to impaired T cell–mediated immune responses. Interestingly, we found that T cells do not infiltrate into the EAE retina (Fig. S8) even though retinal degeneration is observed (47, 48). This indicated that the retina serves as an ideal tissue for studying the role of DOCK8 in microglia without any input by T cells. Therefore, we examined the retina of $DOCK8^{-/-}$ EAE mice. We found that the cell number of RGCs was significantly decreased in WT EAE mice but not in $DOCK8^{-/-}$ EAE mice (Fig. 4A). Consistently, visual function was impaired in WT EAE mice, whereas this impairment was milder in $DOCK8^{-/-}$ EAE mice (Fig. 4B).

Next, we examined a 3D image reconstruction of the retina. Stack images of retinal microglia are displayed in different colors: *red* in the ganglion cell layer (GCL), *green* in the IPL, and *blue* in the OPL (Fig. 4C). In the normal condition, the number of microglia in the GCL was fewer than that in the IPL or OPL (Fig. 4D). In WT EAE mice, the microglial cell number was increased in the GCL, whereas it was decreased in the IPL (Fig. 4, *C and D*). These changes were not detected in $DOCK8^{-/-}$ EAE mice (Fig. 4, *C and D*). These results suggest that microglia migrate from the IPL to the GCL during EAE, and this process is DOCK8-dependent.

### Role of DOCK8 in migration of microglia

We next investigated the role of DOCK8 in migration of microglia. For this, we first examined whether DOCK8 enhances filopodia formation in primary cultured microglia by treatment with cytochalasin D (CyD), a chemical reagent that induced depolymerization of actin filaments, and by detection of filamentous actin (F-actin) filaments with phalloidin. DOCK8 was observed diffusely in the cytoplasm of primary cultured microglia under normal conditions, whereas transient treatment with CyD induced relocalization of DOCK8 from the cytoplasm to the cell periphery where filopodia formation was detected (Fig. 5A, *arrows*). In addition, the number of cells with filopodia, after transient CyD treatment, was reduced in $DOCK8^{-/-}$ microglia compared with WT microglia (Fig. 5B), suggesting that DOCK8 is required for actin assembly in microglia. We next investigated the effects of DOCK8 on microglial cell migration. Using a Boyden chamber assay, we measured the chemotactic response of microglia migration from the control medium (top chamber) toward 10 $\mu$M adenosine triphosphate (ATP; bottom chamber). The motility of WT microglia was increased by ATP attraction, but this increase was significantly lower in $DOCK8^{-/-}$ microglia (Fig. 5C). Altogether, these results indicate that DOCK8 promotes microglial migration via the Cdc42-mediated actin assembly.

### Role of DOCK8 in phagocytosis of microglia

To further confirm the role of microglial DOCK8, we used another model, ONI, an acute model of glaucoma. This model simulates the degeneration of RGCs that occurs in glaucoma, and T cells are not found in the retina (Fig. S8), which gives us an advantage to investigate a role of microglial DOCK8 without the effect of DOCK8 in T cells. Furthermore, microglial activity does not appear to play a role in RGC death in this model (Fig. 6A) (49, 50); this provides a good opportunity to study a role of DOCK8 in phagocytic activity because the level of any signals from dying or dead RGCs is considered to be similar in WT and $DOCK8^{-/-}$ mice. A 3D image reconstruction of the retina revealed that the number of microglia after ONI was strongly increased in the GCL (*red*), IPL (*green*), and OPL (*blue*) in both WT and $DOCK8^{-/-}$ mice (Fig. 6, *B and C*). In WT mice, some dying RGCs were fully wrapped by microglia in the GCL (Fig. 7A). This observation was confirmed by the transverse sequential section images (Fig. 7B) and a 3D image reconstruction (Movie S3) of such cells. The number of phagocytic microglia was reduced in $DOCK8^{-/-}$ mice compared with that in WT mice (Fig. 7C). However, these data are not enough to demonstrate whether there is a difference in phagocytic activity between WT and $DOCK8^{-/-}$ microglia. To examine this point in more detail, we used a dye that fluoresces at an acidic pH such as in phagosomes *in vitro*. We found that phagocytic activity is significantly reduced in $DOCK8^{-/-}$ microglia compared with WT microglia (Fig. 7D).

### Discussion

In this study, we report that DOCK8 is expressed in microglia and is involved in microglial migration and phagocytosis, at least *in vitro*. To the best of our knowledge, this is the first study to show that DOCK8 is expressed in microglia and affects their
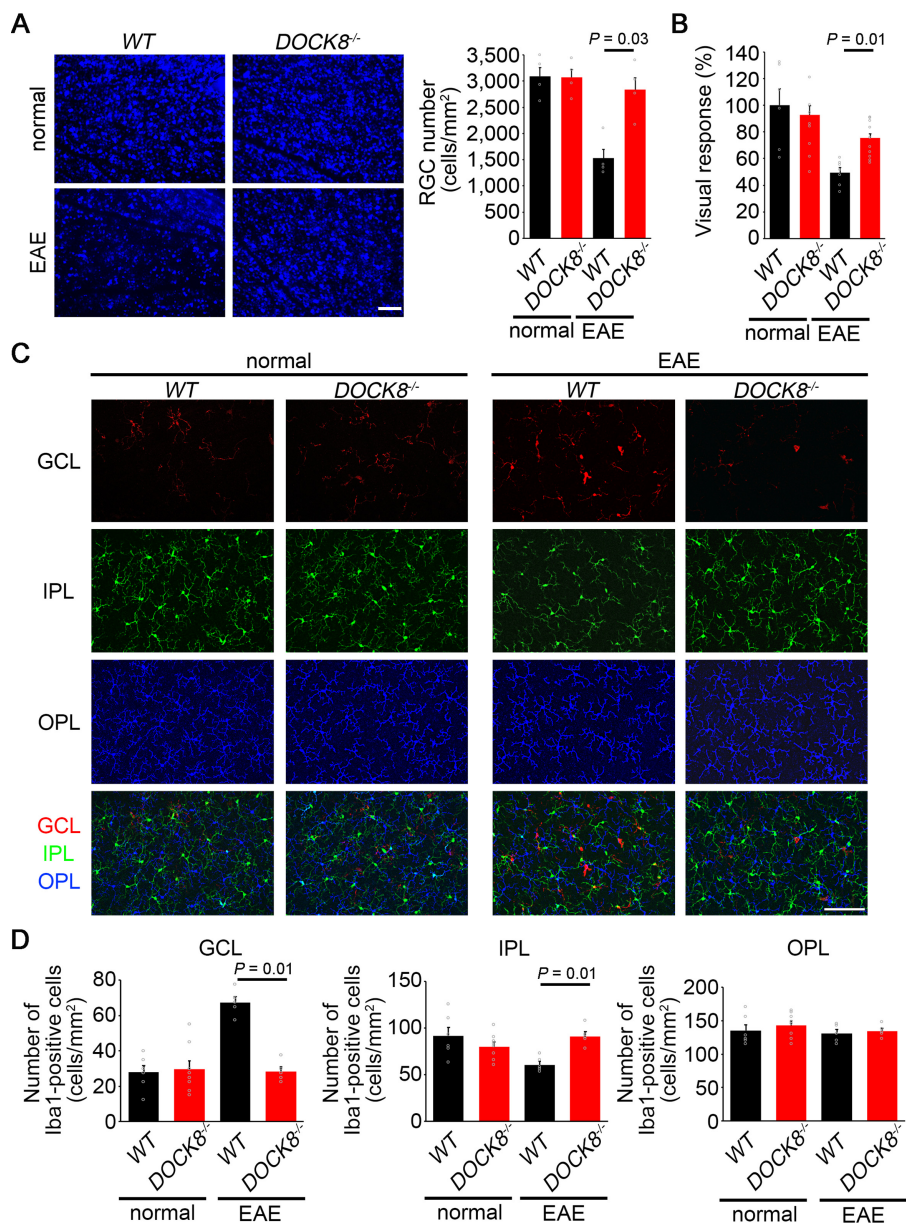
**Figure 4. DOCK8 deficiency preserves visual function and reduces microglial migration in the retinas of EAE mice.** *A*, representative images of FG-labeled RGCs in WT and *DOCK8*$^{-/-}$ EAE mice. FG-labeled RGCs were counted. RGC survival is greatly increased in *DOCK8*$^{-/-}$ EAE mice. *Error bars* represent S.E. (*n* = 4 eyes). *B*, visual responses in WT and *DOCK8*$^{-/-}$ EAE mice by measuring multifocal electroretinogram. The visual responses are better preserved in *DOCK8*$^{-/-}$ EAE mice compared with WT EAE mice. *Error bars* represent S.E. (*n* = 6 eyes for WT normal; *n* = 8 eyes for *DOCK8*$^{-/-}$ normal; *n* = 7 eyes for WT EAE; *n* = 11 eyes for *DOCK8*$^{-/-}$ EAE). *C*, layer-specific microglia distribution in the EAE mouse retina. Microglia were detected by immunostaining of Iba1 in the transparent whole retina. The GCL (*red*), IPL (*green*), OPL (*blue*), and stack images (three layers) of retinal microglia are shown. The Iba1-positive cells are detected in the GCL of WT EAE mice but not in *DOCK8*$^{-/-}$ EAE mice. *Scale bar*, 100 μm. *D*, quantitative analysis of Iba1-positive cells in the GCL, IPL, and OPL. The data suggest that migration from the IPL to the GCL is inhibited in *DOCK8*$^{-/-}$ EAE mice. *Error bars* represent S.E. (*n* = 6 eyes for WT normal; *n* = 8 eyes for *DOCK8*$^{-/-}$ normal; *n* = 5 eyes for WT and *DOCK8*$^{-/-}$ EAE) and data were analyzed by a Mann–Whitney *U* test. *Scale bars*, 100 μm.

activity and to reconstruct 3D images of retinal microglia. The clearing technique we used to reconstruct 3D images of microglia is particularly useful for laminar tissues such as the retina to facilitate the visualization of immunostained cells on different focal plans of the tissue. We demonstrated clear morphological differences in ramified resting microglia in the retina, optic nerve, and spinal cord and in different layers of the retina (Fig. S4, C and D). These differences may simply reflect the available space within the layers, and future studies will include how these shapes affect activities of microglia in disease states.

Microglia play important roles in neuroinflammation, and its migration to the lesion site is necessary for the propagation of neuroinflammation. One of the key events for microglial migration is rearrangement of the actin cytoskeleton by Rho GTPases. Rho GTPases have diverse functions to regulate a variety of cellular processes, including morphogenesis, migration, neuronal development, and cell division (3, 44, 51–53). In particular, Cdc42 plays a crucial role in directing cell migration and chemotaxis (54–56). Our findings indicate that DOCK8 specifically activates Cdc42, and the lack of DOCK8 impairs cell
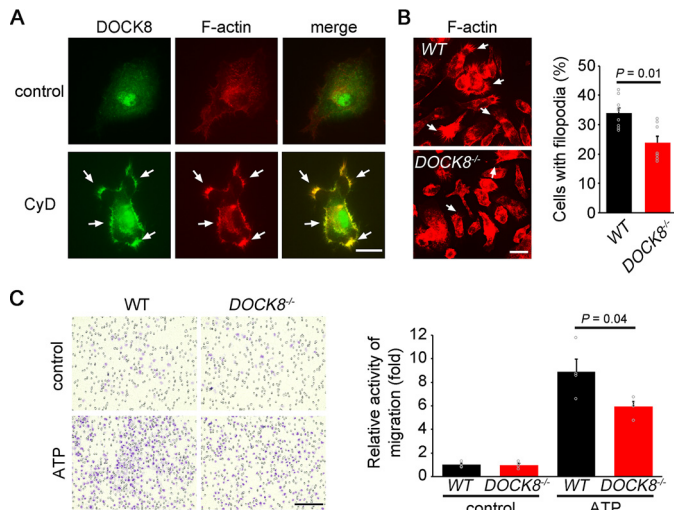
**Figure 5. DOCK8 deficiency impaired microglial migration.** *A*, DOCK8 was colocalized with actin filaments in filopodia (*arrows*) in primary cultured microglia after transient CyD treatment. *B*, filopodia formation (*arrows*) was decreased in *DOCK8−/−* microglia after transient CyD treatment. Cells with filopodia were counted. *Error bars* represent S.E. (*n* = 9 for WT and *n* = 7 for *DOCK8−/−*) and data were analyzed by a Mann–Whitney *U* test. *C*, microglia migration assay using a Boyden chamber. ATP-dependent migration ability was impaired in primary cultured microglia from *DOCK8−/−* mice. *Error bars* represent S.E. (*n* = 4) and data were analyzed by a Mann–Whitney *U* test. *Scale bars*, 10 μm (*A*), 20 μm (*B*), and 100 μm (*C*).

migration, suggesting that the DOCK8–Cdc42 pathway is involved in microglial migration. A recent report indicated that TNFα induces microglial phagocytosis of neurons (57). During ONI, TNFα is elevated, and microglia is activated (42, 58); therefore, it is possible that TNFα up-regulates DOCK8, which promotes phagocytic activity of microglia. Microglial phagocytosis has been implicated in various neurodegenerative diseases, including Alzheimer's disease, Parkinson's disease, ALS, and MS (23, 59–63). However, a role of microglial phagocytosis in disease is complex, and it can act in a beneficial way or in a harmful way, for example, clearing out dead cells and debris or phagocytosing live neurons, respectively (64, 65). Findings from this study alone cannot determine whether microglial phagocytosis is beneficial or harmful during neurodegeneration because microglia have no effects on the severity of RGC death in the ONI model (49, 50), which is an acute model. It has been reported that minocycline suppresses RGC death in animal models of glaucoma (66–68), strongly supporting the role of microglial activation in this disease, and microglia–glia and microglia–neuron interactions may play important roles in the survival or death of retinal neurons (69–71). Future studies will include how microglial DOCK8 affects retinal degeneration in a chronic model of glaucoma (72) and photoreceptor degeneration (69, 70) using microglia-specific *DOCK8−/−* mice. Interestingly, microarray gene expression analysis revealed that DOCK8 is up-regulated in Rett syndrome (73), which is a progressive neurodevelopmental disorder, and its onset and progression may be influenced by microglial activity (74). These findings suggest a role of microglial DOCK8 and its therapeutic potential in some CNS disorders, including MS and glaucoma. In our study, we used *DOCK8−/−* mice to examine a role of DOCK8 in microglial activity during disease. Our results are clear, but we cannot discard the possibility that knocking out a

gene causes compensatory up-regulation of multiple genes, so data from knockout mice may not necessarily be caused by the target gene, in this case *DOCK8*. Therefore, one cannot say for sure that the protective effects observed in this study are due to knocking out *DOCK8* or due to up-regulation of unknown genes as a result of knocking out *DOCK8*.

In summary, we have demonstrated that DOCK8 is expressed in microglia and that it regulates microglial activity during neurodegeneration. Future studies will include generation and use of microglia-specific *DOCK8−/−* mice in disease models to explore the therapeutic potential of microglial DOCK8 in CNS disorders.

## Experimental procedures

### Experimental animals

*DOCK8−/−* mice were generated by homologous recombination in C57BL/6 mouse embryonic stem cells. The animals were treated in accordance with the Tokyo Metropolitan Institute of Medical Science guidelines for the care and use of animals, and all animal experiments were approved by the Institutional Animal Care and Use Committee of the Tokyo Metropolitan Institute of Medical Science.

### Preparation of primary cultured cells

Primary cultured cortical neurons (75, 76), astrocytes (48), microglia, and Müller glia (69, 72) were prepared as described previously. For induction of DOCK8 expression, cultured microglia were stimulated with LPS (10 ng/ml; EMD Millipore, Billerica, MA) or TNFα (50 ng/ml; PeproTech, Rocky Hill, NJ) for 24 h. These cells were directly lysed with a sample buffer (62.5 mM Tris (pH 6.8), 2% SDS, 5% 2-mercaptoethanol, 15% glycerol) and subjected to immunoblotting. For analysis of filopodia formation, cultured microglia were stimulated with 10 μM CyD (EMD Millipore) for 15 min and then washed and cultured in normal culture medium for an additional 15 min. After fixation with 3.7% formaldehyde for 20 min, cells were stained with rhodamine-labeled phalloidin (1:1000; Cytoskeleton, Denver, CO) for visualizing actin filaments.

### Immunostaining of cultured microglia

Primary cultured microglia were fixed with 3.7% formaldehyde for 20 min and stained with 0.03% crystal violet (Fujifilm, Tokyo, Japan) or anti-DOCK8 antibody (1:1000; EMD Millipore). Alexa Fluor–conjugated donkey anti-rabbit IgG (1:1000; Thermo Fisher Scientific, Waltham, MA) was used as a secondary antibody. For visualizing F-actins, cells were stained with rhodamine-labeled phalloidin (1:1000). Cells with or without filopodia were counted manually in two randomly chosen areas of 0.05 mm² per well for a total of 4 wells. Quantitative analysis of the signal bands was carried out using NIH ImageJ software 1.46r.

### Immunoblot analysis

Immunoblotting was carried out as reported previously (75). The optic nerve and spinal cord were freshly isolated from WT and *DOCK8−/−* mice and then homogenized in cold PBS. Total
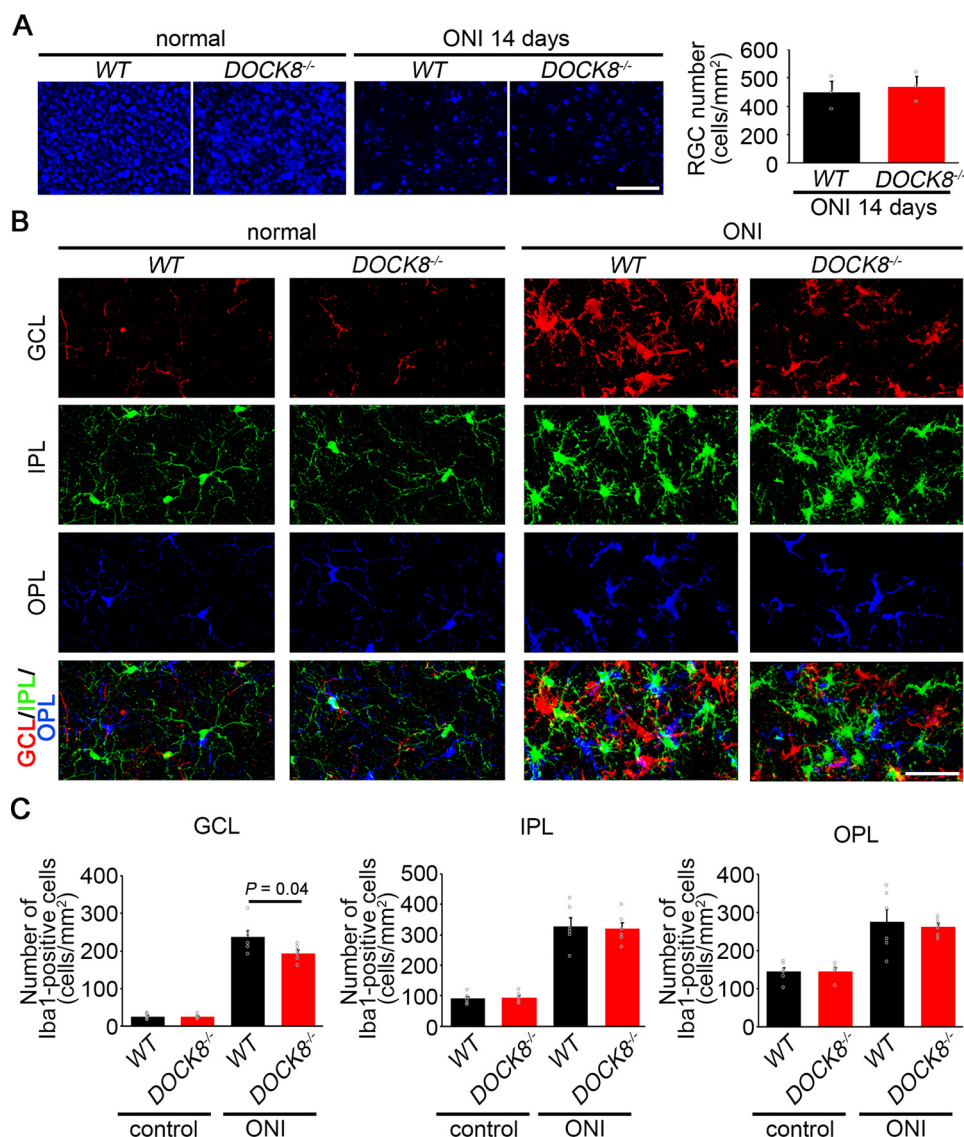
**Figure 6. DOCK8 deficiency reduces microglial migration in the retina following ONI.** *A*, representative images of FG-labeled RGCs in WT and *DOCK8*$^{-/-}$ mice after ONI. FG-labeled RGCs were counted. There was no difference in RGC survival between WT and *DOCK8*$^{-/-}$ mice following ONI. *Error bars* represent S.E. (*n* = 3 eyes). *B*, layer-specific distribution of microglia in mouse retinas 5 days after ONI. Microglia were detected by immunostaining of Iba1 in the transparent whole retina. GCL (*red*), IPL (*green*), OPL (*blue*), and stack images (three layers) of retinal microglia are shown. *C*, quantitative analysis of Iba1-positive cells in the GCL, IPL, and OPL. ONI up-regulates the number of Iba1-positive cells in all retinal layers, but the extent of increase in the GCL is smaller in *DOCK8*$^{-/-}$ mice compared with WT mice. *Error bars* represent S.E. (*n* = 6 eyes) and data were analyzed by a Mann–Whitney *U* test. *Scale bars*, 100 $\mu$m (*A*) and 50 $\mu$m (*B*).

homogenates of the optic nerve and spinal cord or total cell lysates of primary cultured cells were heated at 100 °C for 5 min. Proteins were separated by SDS-PAGE and transferred to an Immobilon-P filter (EMD Millipore). Membranes were incubated with an antibody against DOCK8 (1:1000), Iba1 (1:1000; Abcam, Cambridge, UK), Cdc42 (1:1000; Cell Signaling Technology, Danvers, MA), Rac1 (1:1000; BD Biosciences), RhoA (1:1000; BD Biosciences), Wiskott–Aldrich syndrome protein (WASP) (1:1000; Epitomics, Burlingame, CA), WASP-family verprolin-homologous protein (WAVE) (1:1000; BD Biosciences), and actin (1:1000; BD Biosciences) in PBS containing 0.05% Tween 20 (PBS-T) and 2.5% skimmed milk. Membranes were washed in PBS-T and incubated with horseradish peroxidase–conjugated secondary antibodies against mouse IgG (1:1000; Cell Signaling Technology), rabbit IgG (1:1000; Cell Signaling Technology), or goat IgG (1:1000; Santa Cruz

Biotechnology). Labeled proteins were detected using Chemi-Lumi One Ultra (Nakalai Tesque, Kyoto, Japan). Quantitative analysis of the signal bands was carried out using NIH ImageJ software 1.46r.

### Binding assay for small G proteins

GST-Cdc42, GST-Rac1, and GST-RhoA (84) were purified from bacterial lysates using GSH-agarose (GSH-Sepharose 4B, Thermo Fisher Scientific). After 24 h of transfection with pCMV-full-length DOCK8, COS-7 cells were washed twice with PBS and lysed with an EDTA buffer (1% Triton X-100, 50 mM Tris (pH 7.4), 150 mM NaCl, 5 mM EDTA containing a protease inhibitor mixture (Roche Applied Science)) and centrifuged. The supernatants were incubated with agarose bead–associated GST fusion proteins for 1 h at 4 °C and washed four times. DOCK8 bound to small GTPase proteins was resolved by
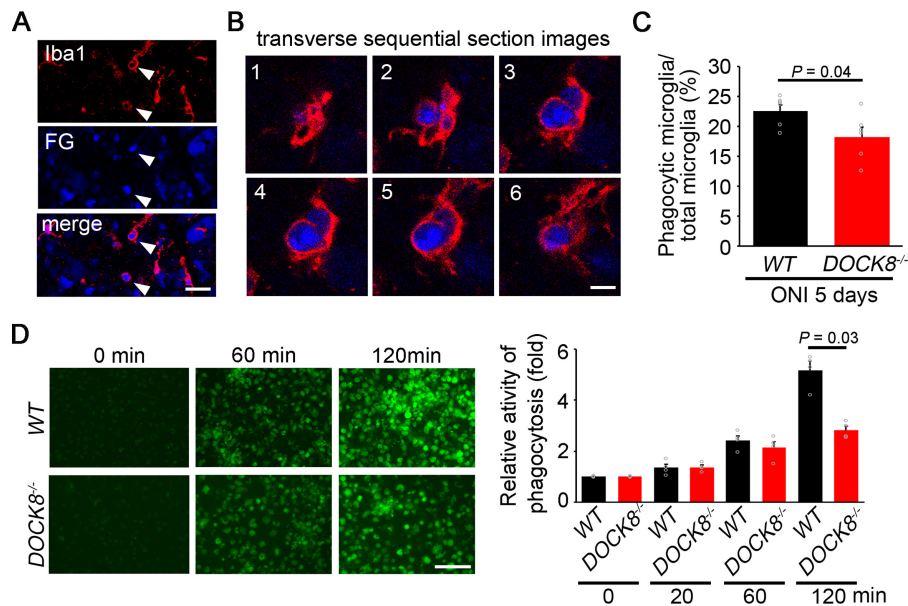
**Figure 7. DOCK8 promotes microglial phagocytosis in the retinas following ONI.** *A*, phagocytic microglia in the transparent whole retina of WT mice 5 days after ONI. The images demonstrate that Iba1-positive cells are wrapping around FG-labeled RGCs (*arrows*). *B*, sequential coronal images of a phagocytic microglial cell in *A*, demonstrating more clearly that the Iba1-positive cell is enveloping the RGC. *C*, quantitative analysis of phagocytic retinal microglia in the GCL. A lesser percentage of phagocytic microglia is found in *DOCK8*$^{-/-}$ mice compared with WT mice. *Error bars* represent S.E. ($n = 6$ eyes) and data were analyzed by a Mann–Whitney $U$ test. *D*, impaired phagocytic ability in *DOCK8*$^{-/-}$ microglia. Microglia were cultured with the fluorescently labeled zymosan particles, which are bright green at an acidic pH such as in phagosomes. The fluorescein intensity was quantified as phagocytic ability. *Error bars* represent S.E. ($n = 4$) and data were analyzed by a Mann–Whitney $U$ test. *Scale bars*, 50 $\mu$m (*A*), 10 $\mu$m (*B*), and 100 $\mu$m (*D*).

SDS-PAGE and assessed by immunoblotting with an anti-DOCK8 antibody (1:1000).

### Measurement of the activity of Rho-family proteins

The activities of Cdc42, Rac1, and RhoA were measured as described previously (75). GST-CRIB and GST-Rhotekin (84) were purified from bacterial lysates using GSH-agarose (Thermo Fisher Scientific). After 24 h of transfection, COS-7 cells were washed twice with PBS and lysed with a lysis buffer (1% Triton X-100, 50 mM Tris (pH 7.4), 150 mM NaCl, 10% glycerol, 10 mM MgCl$_2$ containing protease inhibitor mixture) and then centrifuged. The resulting supernatants were incubated with agarose bead–associated GST fusion proteins for 45 min at 4 °C. The beads were washed four times with lysis buffer, the bound small GTPase proteins were subjected to SDS-PAGE, and immunoblot analysis was performed with anti-Cdc42, -Rac1, and -RhoA antibodies.

### Chemotaxis assay

Migration assays were performed using Boyden-type 96-well plates (ChemoTx system, Neuroprobe, Gaithersburg, MD). Microglia were suspended in Dulbecco's modified Eagle's minimal essential medium without serum. The same medium containing ATP (50 ng/ml; BioVision, Mountain View, CA) was used to fill each well. Polycarbonate filters with 8-$\mu$m pores were placed in contact with the liquid, and cells were dispensed over each well. Cells were seeded on polycarbonate filters and incubated at 37 °C (5% CO$_2$) for 3 h. The cells that remained on the top surface of the filter were wiped with a Kimwipe, and cells under the filter (migrated cells) were fixed with 3.7% formaldehyde for 10 min. The filter was then stained with 0.03% crystal violet, and individual fields were counted.

### Phagocytosis assay

The phagocytic activity was measured using pHrodo™ Green Zymosan Bioparticles™ (Life Technologies) according to the manufacturer's instructions. pHrodo Green conjugates are nonfluorescent outside the cell at a neutral pH but fluoresce brightly green at an acidic pH such as in phagosomes. In brief, microglia were cultured in Dulbecco's modified Eagle's minimal essential medium containing 10% fetal bovine serum and 0.5 mg/ml fluorescently labeled zymosan particles for 20, 60, and 120 min. After fixation, images were obtained with a BZ-9000 fluorescence microscope (Keyence, Osaka, Japan). Fluorescence intensity was determined using NIH ImageJ software 1.46r.

### Histological analyses

Frozen (10-$\mu$m-thick) or paraffin (7-$\mu$m-thick) tissue sections of the retina, optic nerve, or spinal cord were examined with immunohistochemical analysis using anti-Iba1 (1:1000), anti-DOCK8 (1:1000), anti-CD3 (1:1000; Santa Cruz Biotechnology), anti-TREM2 (1:250; Abcam), anti-Ki67 (1:250; Abcam), or anti-glial fibrillary acidic protein (1:1000; Cell Signaling Technology) antibodies. Alexa Fluor–conjugated donkey anti-goat IgG, anti-rabbit IgG, and goat anti-rat IgG (1:1000) were used as secondary antibodies. For detection of myelin in spinal cord, tissues were embedded in paraffin wax, sectioned at a thickness of 7 $\mu$m, and stained with luxol fast blue followed by hematoxylin and eosin. Stained sections were examined using a microscope (BX51, Olympus, Tokyo, Japan) connected to a DP70 camera (Olympus). Images were processed and viewed using DP Manager software (v2.2.1.195; Olympus). Quantitative analysis of the

stained region was carried out using NIH ImageJ software 1.46r.

### Preparation of transparent tissues and immunostaining

Mice were anesthetized by isoflurane and perfused with Zamboni's fixative (2% paraformaldehyde and 15% picric acid in 0.1 M phosphate buffer). Tissues (retina, optic nerve, and spinal cord) were removed and postfixed in Zamboni's fixative for 10 h at 4 °C. The retina and optic nerve as a whole tissue and frozen sections (100 μm) of the spinal cord were immunostained using an anti-Iba1 antibody (1:1000) in 1% Triton X-100, 0.1% SDS, and 5% horse serum in PBS for 2 days at 4 °C with agitation. After washing, tissues were incubated with Alexa Fluor–conjugated donkey anti-goat IgG (1:1000) as a secondary antibody in 1% Triton X-100, 0.1% SDS, and 5% horse serum in PBS for 1 day at 4 °C with agitation. Tissues were then washed and placed on a slide glass with 85% glycerol. Immunostained sequential images were acquired with an SP8 confocal microscope (Leica Microsystems, Wetzlar, Germany) or a BZ-9000 fluorescence microscope. Three-dimensional images were reconstructed with microscope software platform Leica Application Suite X version 1.8 (Leica Microsystems) or ImageJ version 2.0.0 (85).

### Induction and clinical scoring of EAE

Female WT and $DOCK8^{-/-}$ mice were used for the experiments. EAE was induced with the myelin oligodendrocyte glycoprotein $(MOG)_{35-55}$ peptide (MEVGWYRSPFSRVVH-LYRNGK) at 6–8 weeks of age as reported previously (48, 77, 78). To induce EAE, a total of 200 μg of $MOG_{35-55}$ (GenScript, Piscataway, NJ) emulsified in 200 μl of complete Freund's adjuvant (Thermo Fisher Scientific) supplemented with 4 μg/ml *Mycobacterium tuberculosis* was injected subcutaneously into the lower flanks followed by an intraperitoneal injection of 100 ng of pertussis toxin (Thermo Fisher Scientific). Clinical signs were scored daily as follows: 0, no clinical signs; 1, loss of tail tonicity; 2, flaccid tail; 3, impairment of righting reflex; 4, partial hind limb paralysis; 5, complete hind limb paralysis; 6, partial body paralysis; 7, partial forelimb paralysis; 8, complete forelimb paralysis or moribund; 9, death.

### Flow cytometry

Cells were treated with anti-FcγRII/III (BioLegend, San Diego, CA) to block unspecific binding to Fc receptors and thereafter labeled with fluorescent antibodies for flow cytometric acquisition using a FACSCalibur flow cytometer. Data analysis was performed by Flowjo software (Treestar, Ashland, OR). The following antibodies were used for surface staining of splenocytes: Alexa Fluor 488–conjugated anti-CD3 (BioLegend), phycoerythrin-conjugated anti-CD4 (BioLegend), and Alexa Fluor 647–conjugated anti-CD8a (BioLegend).

### Antigen-specific T-cell proliferation assay

Bone marrow–derived dendritic cells (BMDCs) were prepared according to previously reported methods with slight modifications (79). Bone marrow was isolated from the femurs and tibias of WT and $DOCK8^{-/-}$ mice. Bone marrow cells ($5 \times 10^6$) were resuspended in 10 ml of dendritic cell (DC) medium

(RPMI 1640 medium (Nakalai), 10% fetal calf serum, 10 ng/ml granulocyte/macrophage colony-stimulating factor (Pepro-Tech)) and cultured in 10-cm culture dishes at 37 °C. Three days after cell culture, 10 ml of DC medium was added to the culture. Six days after cell culture, 10 ml of the culture was removed and centrifuged, and the cell pellet was resuspended in 10 ml of fresh DC medium and added back to the culture. Nine days after cell culture, BMDCs were harvested, pulsed for 2 h with ovalbumin (100 μg/ml; EMD Millipore), and washed prior to use in *in vitro* proliferation assays. Additionally, splenocytes of OT-II transgenic mice (80) were isolated and stained with 5-(and-6)-carboxyfluorescein diacetate succinimidyl ester (CFSE; final concentration, 0.5 μM; Dojindo, Kumamoto, Japan). CFSE-labeled OT-II splenocytes ($4 \times 10^5$) were cocultured with ovalbumin-pulsed BMDCs ($1 \times 10^5$) in 96-well round-bottom plates and incubated for 3 days at 37 °C. After culture, the cells were stained with an anti-CD4 mAb (1:1500; BioLegend) and analyzed by flow cytometry to detect CFSE dilution of gated $CD4^+$ OT-II T cells.

### Analysis of complete blood cells

Peripheral blood was obtained by tail bleeding and transferred into EDTA-coated tubes. The complete blood cell analysis was performed using a Sysmex K-4500 multispecies whole-blood analyzer (Sysmex, Kobe, Japan).

### Multifocal electroretinograms

Mice were anesthetized by intraperitoneal injection of 87.5 mg/kg sodium pentobarbital. The pupils were dilated with 0.5% phenylephrine hydrochloride and 0.5% tropicamide. Multifocal electroretinograms were recorded using a VERIS 6.0 system (Electro-Diagnostic Imaging, Redwood City, CA). The visual stimulus consisted of seven hexagonal areas scaled with eccentricity. The stimulus array was displayed on a high-resolution black and white monitor driven at a frame rate of 100 Hz. The second-order kernel, which is impaired in optic neuritis and optic neuropathy, was analyzed (48, 72, 81).

### Retrograde RGC labeling

Mice were deeply anesthetized with isoflurane and then placed on a stereotaxic frame before receiving an injection of 2 μl of 1% Fluoro-Gold (FG; Fluorochrome LLC, Denver, CO) dissolved in PBS into the superior colliculus (82, 83). Ten days after FG application, mice were anesthetized, eyes were enucleated, and retinas were isolated for whole-mount preparation. Retinas were fixed in 4% paraformaldehyde in 0.1 M PBS solution for 20 min and mounted on a glass slide with a mounting medium (Vectashield, Vector Laboratories, Burlingame, CA), and RGC density was examined with a fluorescence microscope. The excitation and emission wavelengths for FG were 323 and 620 nm, respectively. Four standard areas (0.1 mm²) of each retina at a point 0.5 mm from the optic disc were chosen. FG-labeled cells were manually counted, and the mean number of RGCs per mm² was calculated.

### ONI

Mice were anesthetized with isoflurane before ONI. Optic nerves were exposed intraorbitally and crushed about 0.5-1.0

mm from the posterior pole of the eyeball with fine surgical forceps for 5 s (75). Five days after ONI, eyes were enucleated, and isolated retinas were processed for tissue clearing and immunostaining. In some experiments, retrograde RGC labeling was carried out 10 days before ONI.

### Immunostaining of human brain

Human samples were handled according to the regulations issued by the Ethics Committee of the Tokyo Metropolitan Institute of Medical Science. This study was conducted in accordance with Declaration of Helsinki principles. CNS tissues were obtained at autopsy from a 54-year-old male (Patient 1), 40-year-old female (Patient 2), and 56-year-old male (Patient 3) whose disease status was relapsing–remitting MS. The tissue was fixed with 20% buffered formalin and embedded in paraffin wax. For immunohistochemistry, 10-$\mu$m paraffin sections were immunostained using a rabbit polyclonal antibody against DOCK8 (1:1000). Before antibody incubation, sections were heated using a microwave in citrate-buffered saline (pH 6.0) for 15 min to unmask antigens. Antibody binding was visualized using a labeled streptavidin–biotin immunoperoxidase method.

### Statistical analyses

Data are presented as means $\pm$ S.E. Data were analyzed by a two-tailed unpaired Student's $t$ test or Mann–Whitney $U$ test as a nonparametric test, and the $p$ values were not corrected for multiple comparisons. A value of $p < 0.05$ was regarded as statistically significant. JMP, version 8.0.1 (SAS Institute, Cary, NC) was used for the statistical analyses.

### References

1. Ruusala, A., and Aspenström, P. (2004) Isolation and characterisation of DOCK8, a member of the DOCK180-related regulators of cell morphology. *FEBS Lett.* **572,** 159–166 CrossRef Medline
2. Côté, J. F., and Vuori, K. (2007) GEF what? Dock180 and related proteins help Rac to polarize cells in new ways. *Trends Cell Biol.* **17,** 383–393 CrossRef Medline
3. Hall, A. (2012) Rho family GTPases. *Biochem. Soc. Trans.* **40,** 1378–1382 CrossRef Medline
4. Laurin, M., and Côté, J. F. (2014) Insights into the biological functions of Dock family guanine nucleotide exchange factors. *Genes Dev.* **28,** 533–547 CrossRef Medline
5. Namekata, K., Kimura, A., Kawamura, K., Harada, C., and Harada, T. (2014) Dock GEFs and their therapeutic potential: neuroprotection and axon regeneration. *Prog. Retin. Eye Res.* **43,** 1–16 CrossRef Medline
6. Zhang, Q., Davis, J. C., Lamborn, I. T., Freeman, A. F., Jing, H., Favreau, A. J., Matthews, H. F., Davis, J., Turner, M. L., Uzel, G., Holland, S. M., and Su, H. C. (2009) Combined immunodeficiency associated with DOCK8 mutations. *N. Engl. J. Med.* **361,** 2046–2055 CrossRef Medline
7. Engelhardt, K. R., McGhee, S., Winkler, S., Sassi, A., Woellner, C., Lopez-Herrera, G., Chen, A., Kim, H. S., Lloret, M. G., Schulze, I., Ehl, S., Thiel, J., Pfeifer, D., Veelken, H., Niehues, T., *et al.* (2009) Large deletions and point mutations involving the dedicator of cytokinesis 8 (DOCK8) in the auto-

8. Su, H. C., Jing, H., and Zhang, Q. (2011) DOCK8 deficiency. *Ann. N.Y. Acad. Sci.* **1246,** 26–33 CrossRef Medline
9. Tirosh, O., Conlan, S., Deming, C., Lee-Lin, S. Q., Huang, X., NISC Comparative Sequencing Program, Su, H. C., Freeman, A. F., Segre, J. A., and Kong, H. H. (2018) Expanded skin virome in DOCK8-deficient patients. *Nat. Med.* **24,** 1815–1821 CrossRef Medline
10. Randall, K. L., Lambe, T., Johnson, A., Treanor, B., Kucharska, E., Domaschenz, H., Whittle, B., Tze, L. E., Enders, A., Crockford, T. L., Bouriez-Jones, T., Alston, D., Cyster, J. G., Lenardo, M. J., Mackay, F., *et al.* (2009) Dock8 mutations cripple B cell immunological synapses, germinal centers and long-lived antibody production. *Nat. Immunol.* **10,** 1283–1291 CrossRef Medline
11. Jabara, H. H., McDonald, D. R., Janssen, E., Massaad, M. J., Ramesh, N., Borzutzky, A., Rauter, I., Benson, H., Schneider, L., Baxi, S., Recher, M., Notarangelo, L. D., Wakim, R., Dbaibo, G., Dasouki, M., *et al.* (2012) DOCK8 functions as an adaptor that links TLR-MyD88 signaling to B cell activation. *Nat. Immunol.* **13,** 612–620 CrossRef Medline
12. Randall, K. L., Chan, S. S., Ma, C. S., Fung, I., Mei, Y., Yabas, M., Tan, A., Arkwright, P. D., Al Suwairi, W., Lugo Reyes, S. O., Yamazaki-Nakashimada, M. A., Garcia-Cruz Mde, L., Smart, J. M., Picard, C., Okada, S., *et al.* (2011) DOCK8 deficiency impairs CD8 T cell survival and function in humans and mice. *J. Exp. Med.* **208,** 2305–2320 CrossRef Medline
13. Crawford, G., Enders, A., Gileadi, U., Stankovic, S., Zhang, Q., Lambe, T., Crockford, T. L., Lockstone, H. E., Freeman, A., Arkwright, P. D., Smart, J. M., Ma, C. S., Tangye, S. G., Goodnow, C. C., Cerundolo, V., *et al.* (2013) DOCK8 is critical for the survival and function of NKT cells. *Blood* **122,** 2052–2061 CrossRef Medline
14. Zhang, Q., Dove, C. G., Hor, J. L., Murdock, H. M., Strauss-Albee, D. M., Garcia, J. A., Mandl, J. N., Grodick, R. A., Jing, H., Chandler-Brown, D. B., Lenardo, T. E., Crawford, G., Matthews, H. F., Freeman, A. F., Cornall, R. J., *et al.* (2014) DOCK8 regulates lymphocyte shape integrity for skin antiviral immunity. *J. Exp. Med.* **211,** 2549–2566 CrossRef Medline
15. Yamamura, K., Uruno, T., Shiraishi, A., Tanaka, Y., Ushijima, M., Nakahara, T., Watanabe, M., Kido-Nakahara, M., Tsuge, I., Furue, M., and Fukui, Y. (2017) The transcription factor EPAS1 links DOCK8 deficiency to atopic skin inflammation via IL-31 induction. *Nat. Commun.* **8,** 13946 CrossRef Medline
16. Janssen, E., Tohme, M., Hedayat, M., Leick, M., Kumari, S., Ramesh, N., Massaad, M. J., Ullas, S., Azcutia, V., Goodnow, C. C., Randall, K. L., Qiao, Q., Wu, H., Al-Herz, W., Cox, D., *et al.* (2016) A DOCK8-WIP-WASp complex links T cell receptors to the actin cytoskeleton. *J. Clin. Investig.* **126,** 3837–3851 CrossRef Medline
17. Harada, Y., Tanaka, Y., Terasawa, M., Pieczyk, M., Habiro, K., Katakai, T., Hanawa-Suetsugu, K., Kukimoto-Niino, M., Nishizaki, T., Shirouzu, M., Duan, X., Uruno, T., Nishikimi, A., Sanematsu, F., Yokoyama, S., *et al.* (2012) DOCK8 is a Cdc42 activator critical for interstitial dendritic cell migration during immune responses. *Blood* **119,** 4451–4461 CrossRef Medline
18. Krishnaswamy, J. K., Singh, A., Gowthaman, U., Wu, R., Gorrepati, P., Sales Nascimento, M., Gallman, A., Liu, D., Rhebergen, A. M., Calabro, S., Xu, L., Ranney, P., Srivastava, A., Ranson, M., Gorham, J. D., *et al.* (2015) Coincidental loss of DOCK8 function in NLRP10-deficient and C3H/HeJ mice results in defective dendritic cell migration. *Proc. Natl. Acad. Sci. U.S.A.* **112,** 3056–3061 CrossRef Medline
19. Vinci, G., Chantot-Bastaraud, S., El Houate, B., Lortat-Jacob, S., Brauner, R., and McElreavey, K. (2007) Association of deletion 9p, 46, XY gonadal dysgenesis and autistic spectrum disorder. *Mol. Hum. Reprod.* **13,** 685–689 CrossRef Medline
20. Griggs, B. L., Ladd, S., Saul, R. A., DuPont, B. R., and Srivastava, A. K. (2008) Dedicator of cytokinesis 8 is disrupted in two patients with mental retardation and developmental disabilities. *Genomics* **91,** 195–202 CrossRef Medline
21. Schramm, A., Köster, J., Assenov, Y., Althoff, K., Peifer, M., Mahlow, E., Odersky, A., Beisser, D., Ernst, C., Henssen, A. G., Stephan, H., Schröder, C., Heukamp, L., Engesser, A., Kahlert, Y., *et al.* (2015) Mutational dynam-

ics between primary and relapse neuroblastomas. *Nat. Genet.* **47,** 872–877 CrossRef Medline

22. Dheen, S. T., Kaur, C., and Ling, E. A. (2007) Microglial activation and its implications in the brain diseases. *Curr. Med. Chem.* **14,** 1189–1197 CrossRef Medline

23. Salter, M. W., and Stevens, B. (2017) Microglia emerge as central players in brain disease. *Nat. Med.* **23,** 1018–1027 CrossRef Medline

24. Heneka, M. T., Carson, M. J., El Khoury, J., Landreth, G. E., Brosseron, F., Feinstein, D. L., Jacobs, A. H., Wyss-Coray, T., Vitorica, J., Ransohoff, R. M., Herrup, K., Frautschy, S. A., Finsen, B., Brown, G. C., Verkhratsky, A., *et al.* (2015) Neuroinflammation in Alzheimer's disease. *Lancet Neurol.* **14,** 388–405 CrossRef Medline

25. Inoue, K., and Tsuda, M. (2018) Microglia in neuropathic pain: cellular and molecular mechanisms and therapeutic potential. *Nat. Rev. Neurosci.* **19,** 138–152 CrossRef Medline

26. Constantinescu, C. S., Farooqi, N., O'Brien, K., and Gran, B. (2011) Experimental autoimmune encephalomyelitis (EAE) as a model for multiple sclerosis (MS). *Br. J. Pharmacol.* **164,** 1079–1106 CrossRef Medline

27. Ransohoff, R. M. (2012) Animal models of multiple sclerosis: the good, the bad and the bottom line. *Nat. Neurosci.* **15,** 1074–1077 CrossRef Medline

28. Steinman, L. (1996) Multiple sclerosis: a coordinated immunological attack against myelin in the central nervous system. *Cell* **85,** 299–302 CrossRef Medline

29. Weiner, H. L. (2004) Multiple sclerosis is an inflammatory T-cell-mediated autoimmune disease. *Arch. Neurol.* **61,** 1613–1615 CrossRef Medline

30. Korn, T. (2008) Pathophysiology of multiple sclerosis. *J. Neurol.* **255,** Suppl. 6, 2–6 CrossRef Medline

31. Baeten, D. L., and Kuchroo, V. K. (2013) How cytokine networks fuel inflammation: interleukin-17 and a tale of two autoimmune diseases. *Nat. Med.* **19,** 824–825 CrossRef Medline

32. Muramatsu, R., Kubo, T., Mori, M., Nakamura, Y., Fujita, Y., Akutsu, T., Okuno, T., Taniguchi, J., Kumanogoh, A., Yoshida, M., Mochizuki, H., Kuwabara, S., and Yamashita, T. (2011) RGMa modulates T cell responses and is involved in autoimmune encephalomyelitis. *Nat. Med.* **17,** 488–494 CrossRef Medline

33. Guo, X., Nakamura, K., Kohyama, K., Harada, C., Behanna, H. A., Watterson, D. M., Matsumoto, Y., and Harada, T. (2007) Inhibition of glial cell activation ameliorates the severity of experimental autoimmune encephalomyelitis. *Neurosci. Res.* **59,** 457–466 CrossRef Medline

34. Guo, X., Harada, C., Namekata, K., Matsuzawa, A., Camps, M., Ji, H., Swinnen, D., Jorand-Lebrun, C., Muzerelle, M., Vitte, P. A., Rückle, T., Kimura, A., Kohyama, K., Matsumoto, Y., Ichijo, H., *et al.* (2010) Regulation of the severity of neuroinflammation and demyelination by TLR-ASK1-p38 pathway. *EMBO Mol. Med.* **2,** 504–515 CrossRef Medline

35. Rasmussen, S., Wang, Y., Kivisäkk, P., Bronson, R. T., Meyer, M., Imitola, J., and Khoury, S. J. (2007) Persistent activation of microglia is associated with neuronal dysfunction of callosal projecting pathways and multiple sclerosis-like lesions in relapsing–remitting experimental autoimmune encephalomyelitis. *Brain* **130,** 2816–2829 CrossRef Medline

36. Goldmann, T., and Prinz, M. (2013) Role of microglia in CNS autoimmunity. *Clin. Dev. Immunol.* **2013,** 208093 CrossRef Medline

37. Peterson, J. W., Bö, L., Mörk, S., Chang, A., and Trapp, B. D. (2001) Transected neurites, apoptotic neurons, and reduced inflammation in cortical multiple sclerosis lesions. *Ann. Neurol.* **50,** 389–400 CrossRef Medline

38. Metz, L. M., Li, D. K. B., Traboulsee, A. L., Duquette, P., Eliasziw, M., Cerchiaro, G., Greenfield, J., Riddehough, A., Yeung, M., Kremenchutzky, M., Vorobeychik, G., Freedman, M. S., Bhan, V., Blevins, G., Marriott, J. J., *et al.* (2017) Trial of minocycline in a clinically isolated syndrome of multiple sclerosis. *N. Engl. J. Med.* **376,** 2122–2133 CrossRef Medline

39. Karlstetter, M., Scholz, R., Rutar, M., Wong, W. T., Provis, J. M., and Langmann, T. (2015) Retinal microglia: just bystander or target for therapy? *Prog. Retin. Eye Res.* **45,** 30–57 CrossRef Medline

40. Thanos, S. (1991) The relationship of microglial cells to dying neurons during natural neuronal cell death and axotomy-induced degeneration of the rat retina. *Eur. J. Neurosci.* **3,** 1189–1207 CrossRef Medline

41. Sobrado-Calvo, P., Vidal-Sanz, M., and Villegas-Pérez, M. P. (2007) Rat retinal microglial cells under normal conditions, after optic nerve section, and after optic nerve section and intravitreal injection of trophic factors or macrophage inhibitory factor. *J. Comp. Neurol.* **501,** 866–878 CrossRef Medline

42. Katome, T., Namekata, K., Guo, X., Semba, K., Kittaka, D., Kawamura, K., Kimura, A., Harada, C., Ichijo, H., Mitamura, Y., and Harada, T. (2013) Inhibition of ASK1-p38 pathway prevents neural cell death following optic nerve injury. *Cell Death Differ.* **20,** 270–280 CrossRef Medline

43. Noro, T., Namekata, K., Kimura, A., Guo, X., Azuchi, Y., Harada, C., Nakano, T., Tsuneoka, H., and Harada, T. (2015) Spermidine promotes retinal ganglion cell survival and optic nerve regeneration in adult mice following optic nerve injury. *Cell Death Dis.* **6,** e1720 CrossRef Medline

44. Raftopoulou, M., and Hall, A. (2004) Cell migration: Rho GTPases lead the way. *Dev. Biol.* **265,** 23–32 CrossRef Medline

45. Forabosco, P., Ramasamy, A., Trabzuni, D., Walker, R., Smith, C., Bras, J., Levine, A. P., Hardy, J., Pocock, J. M., Guerreiro, R., Weale, M. E., and Ryten, M. (2013) Insights into TREM2 biology by network analysis of human brain gene expression data. *Neurobiol. Aging* **34,** 2699–2714 CrossRef Medline

46. Xu, X., Han, L., Zhao, G., Xue, S., Gao, Y., Xiao, J., Zhang, S., Chen, P., Wu, Z. Y., Ding, J., Hu, R., Wei, B., and Wang, H. (2017) LRCH1 interferes with DOCK8-Cdc42-induced T cell migration and ameliorates experimental autoimmune encephalomyelitis. *J. Exp. Med.* **214,** 209–226 CrossRef Medline

47. Guo, X., Harada, C., Namekata, K., Kikushima, K., Mitamura, Y., Yoshida, H., Matsumoto, Y., and Harada, T. (2009) Effect of geranylgeranylacetone on optic neuritis in experimental autoimmune encephalomyelitis. *Neurosci. Lett.* **462,** 281–285 CrossRef Medline

48. Guo, X., Harada, C., Namekata, K., Kimura, A., Mitamura, Y., Yoshida, H., Matsumoto, Y., and Harada, T. (2011) Spermidine alleviates severity of murine experimental autoimmune encephalomyelitis. *Invest. Ophthalmol. Vis. Sci.* **52,** 2696–2703 CrossRef Medline

49. Liddelow, S. A., Guttenplan, K. A., Clarke, L. E., Bennett, F. C., Bohlen, C. J., Schirmer, L., Bennett, M. L., Münch, A. E., Chung, W. S., Peterson, T. C., Wilton, D. K., Frouin, A., Napier, B. A., Panicker, N., Kumar, M., *et al.* (2017) Neurotoxic reactive astrocytes are induced by activated microglia. *Nature* **541,** 481–487 CrossRef Medline

50. Hilla, A. M., Diekmann, H., and Fischer, D. (2017) Microglia are irrelevant for neuronal degeneration and axon regeneration after acute injury. *J. Neurosci.* **37,** 6113–6124 CrossRef Medline

51. Heasman, S. J., and Ridley, A. J. (2008) Mammalian Rho GTPases: new insights into their functions from *in vivo* studies. *Nat. Rev. Mol. Cell Biol.* **9,** 690–701 CrossRef Medline

52. Hall, A., and Lalli, G. (2010) Rho and Ras GTPases in axon growth, guidance, and branching. *Cold Spring Harb. Perspect. Biol.* **2,** a001818 CrossRef Medline

53. Cook, D. R., Rossman, K. L., and Der, C. J. (2014) Rho guanine nucleotide exchange factors: regulators of Rho GTPase activity in development and disease. *Oncogene* **33,** 4021–4035 CrossRef Medline

54. Yang, L., Wang, L., and Zheng, Y. (2006) Gene targeting of Cdc42 and Cdc42GAP affirms the critical involvement of Cdc42 in filopodia induction, directed migration, and proliferation in primary mouse embryonic fibroblasts. *Mol. Biol. Cell* **17,** 4675–4685 CrossRef Medline

55. Ridley, A. J. (2015) Rho GTPase signalling in cell migration. *Curr. Opin. Cell Biol.* **36,** 103–112 CrossRef Medline

56. Yang, H. W., Collins, S. R., and Meyer, T. (2016) Locally excitable Cdc42 signals steer cells during chemotaxis. *Nat. Cell Biol.* **18,** 191–201 CrossRef Medline

57. Neniskyte, U., Vilalta, A., and Brown, G. C. (2014) Tumour necrosis factor α-induced neuronal loss is mediated by microglial phagocytosis. *FEBS Lett.* **588,** 2952–2956 CrossRef Medline

58. Harada, C., Azuchi, Y., Noro, T., Guo, X., Kimura, A., Namekata, K., and Harada, T. (2015) TrkB signaling in retinal glia stimulates neuroprotection after optic nerve injury. *Am. J. Pathol.* **185,** 3238–3247 CrossRef Medline

59. Koenigsknecht-Talboo, J., and Landreth, G. E. (2005) Microglial phagocytosis induced by fibrillar β-amyloid and IgGs are differentially regulated by proinflammatory cytokines. *J. Neurosci.* **25,** 8240–8249 CrossRef Medline

60. Park, J. Y., Paik, S. R., Jou, I., and Park, S. M. (2008) Microglial phagocytosis is enhanced by monomeric α-synuclein, not aggregated α-synuclein: implications for Parkinson's disease. *Glia* **56,** 1215–1223 CrossRef Medline

61. Sanagi, T., Yuasa, S., Nakamura, Y., Suzuki, E., Aoki, M., Warita, H., Itoyama, Y., Uchino, S., Kohsaka, S., and Ohsawa, K. (2010) Appearance of phagocytic microglia adjacent to motoneurons in spinal cord tissue from a presymptomatic transgenic rat model of amyotrophic lateral sclerosis. *J. Neurosci. Res.* **88,** 2736–2746 CrossRef Medline

62. Neumann, H., Kotter, M. R., and Franklin, R. J. (2009) Debris clearance by microglia: an essential link between degeneration and regeneration. *Brain* **132,** 288–295 CrossRef Medline

63. Fu, R., Shen, Q., Xu, P., Luo, J. J., and Tang, Y. (2014) Phagocytosis of microglia in the central nervous system diseases. *Mol. Neurobiol.* **49,** 1422–1434 CrossRef Medline

64. Neher, J. J., Neniskyte, U., and Brown, G. C. (2012) Primary phagocytosis of neurons by inflamed microglia: potential roles in neurodegeneration. *Front. Pharmacol.* **3,** 27 CrossRef Medline

65. Brown, G. C., and Neher, J. J. (2014) Microglial phagocytosis of live neurons. *Nat. Rev. Neurosci.* **15,** 209–216 CrossRef Medline

66. Shimazawa, M., Yamashima, T., Agarwal, N., and Hara, H. (2005) Neuroprotective effects of minocycline against *in vitro* and *in vivo* retinal ganglion cell damage. *Brain Res.* **1053,** 185–194 CrossRef Medline

67. Baptiste, D. C., Powell, K. J., Jollimore, C. A., Hamilton, C., LeVatte, T. L., Archibald, M. L., Chauhan, B. C., Robertson, G. S., and Kelly, M. E. (2005) Effects of minocycline and tetracycline on retinal ganglion cell survival after axotomy. *Neuroscience* **134,** 575–582 CrossRef Medline

68. Bosco, A., Inman, D. M., Steele, M. R., Wu, G., Soto, I., Marsh-Armstrong, N., Hubbard, W. C., Calkins, D. J., Horner, P. J., and Vetter, M. L. (2008) Reduced retina microglial activation and improved optic nerve integrity with minocycline treatment in the DBA/2J mouse model of glaucoma. *Invest. Ophthalmol. Vis. Sci.* **49,** 1437–1446 CrossRef Medline

69. Harada, T., Harada, C., Kohsaka, S., Wada, E., Yoshida, K., Ohno, S., Mamada, H., Tanaka, K., Parada, L. F., and Wada, K. (2002) Microglia-Müller glia cell interactions control neurotrophic factor production during light-induced retinal degeneration. *J. Neurosci.* **22,** 9228–9236 CrossRef Medline

70. Harada, C., Guo, X., Namekata, K., Kimura, A., Nakamura, K., Tanaka, K., Parada, L. F., and Harada, T. (2011) Glia- and neuron-specific functions of TrkB signalling during retinal degeneration and regeneration. *Nat. Commun.* **2,** 189 CrossRef Medline

71. Vecino, E., Rodriguez, F. D., Ruzafa, N., Pereiro, X., and Sharma, S. C. (2016) Glia-neuron interactions in the mammalian retina. *Prog. Retin. Eye Res.* **51,** 1–40 CrossRef Medline

72. Harada, T., Harada, C., Nakamura, K., Quah, H. M., Okumura, A., Namekata, K., Saeki, T., Aihara, M., Yoshida, H., Mitani, A., and Tanaka, K. (2007) The potential role of glutamate transporters in the pathogenesis of normal tension glaucoma. *J. Clin. Investig.* **117,** 1763–1770 CrossRef Medline

73. Orlic-Milacic, M., Kaufman, L., Mikhailov, A., Cheung, A. Y., Mahmood, H., Ellis, J., Gianakopoulos, P. J., Minassian, B. A., and Vincent, J. B. (2014) Over-expression of either MECP2_e1 or MECP2_e2 in neuronally differentiated cells results in different patterns of gene expression. *PLoS One* **9,** e91742 CrossRef Medline

74. Maezawa, I., and Jin, L. W. (2010) Rett syndrome microglia damage dendrites and synapses by the elevated release of glutamate. *J. Neurosci.* **30,** 5346–5356 CrossRef Medline

75. Namekata, K., Harada, C., Taya, C., Guo, X., Kimura, H., Parada, L. F., and Harada, T. (2010) Dock3 induces axonal outgrowth by stimulating membrane recruitment of the WAVE complex. *Proc. Natl. Acad. Sci. U.S.A.* **107,** 7586–7591 CrossRef Medline

76. Namekata, K., Harada, C., Guo, X., Kimura, A., Kittaka, D., Watanabe, H., and Harada, T. (2012) Dock3 stimulates axonal outgrowth via GSK-3β-mediated microtubule assembly. *J. Neurosci.* **32,** 264–274 CrossRef Medline

77. Mendel, I., Kerlero de Rosbo, N., and Ben-Nun, A. (1995) A myelin oligodendrocyte glycoprotein peptide induces typical chronic experimental autoimmune encephalomyelitis in H-2b mice: fine specificity and T cell receptor V β expression of encephalitogenic T cells. *Eur. J. Immunol.* **25,** 1951–1959 CrossRef Medline

78. Guo, X., Namekata, K., Kimura, A., Harada, C., and Harada, T. (2017) The renin-angiotensin system regulates neurodegeneration in a mouse model of optic neuritis. *Am. J. Pathol.* **187,** 2876–2885 CrossRef Medline

79. Lutz, M. B., Kukutsch, N., Ogilvie, A. L., Rössner, S., Koch, F., Romani, N., and Schuler, G. (1999) An advanced culture method for generating large quantities of highly pure dendritic cells from mouse bone marrow. *J. Immunol. Methods* **223,** 77–92 CrossRef Medline

80. Barnden, M. J., Allison, J., Heath, W. R., and Carbone, F. R. (1998) Defective TCR expression in transgenic mice constructed using cDNA-based α- and β-chain genes under the control of heterologous regulatory elements. *Immunol. Cell Biol.* **76,** 34–40 CrossRef Medline

81. Sutter, E. E., and Bearse, M. A., Jr. (1999) The optic nerve head component of the human ERG. *Vision Res.* **39,** 419–436 CrossRef Medline

82. Harada, C., Nakamura, K., Namekata, K., Okumura, A., Mitamura, Y., Iizuka, Y., Kashiwagi, K., Yoshida, K., Ohno, S., Matsuzawa, A., Tanaka, K., Ichijo, H., and Harada, T. (2006) Role of apoptosis signal-regulating kinase 1 in stress-induced neural cell apoptosis *in vivo*. *Am. J. Pathol.* **168,** 261–269 CrossRef Medline

83. Akaiwa, K., Namekata, K., Azuchi, Y., Guo, X., Kimura, A., Harada, C., Mitamura, Y., and Harada, T. (2017) Edaravone suppresses retinal ganglion cell death in a mouse model of normal tension glaucoma. *Cell Death Dis.* **8,** e2934 CrossRef Medline

84. Namekata, K., Enokido, Y., Iwasawa, K., and Kimura, H. (2004) MOCA induces membrane spreading by activating Rac1. *J. Biol. Chem.* **279,** 14331–14337 CrossRef Medline

85. Schindelin, J., Arganda-Carreras, I., Frise, E., Kaynig, V., Longair, M., Pietzsch, T., Preibisch, S., Rueden, C., Saalfeld, S., Schmid, B., Tinevez, J. Y., White, D. J., Hartenstein, V., Eliceiri, K., Tomancak, P., *et al.* (2012) Fiji: an open-source platform for biological-image analysis. *Nat. Methods* **9,** 676–682 CrossRef Medline